

# A new assay capturing chromosome fusions shows a protection trade-off at telomeres and NHEJ vulnerability to low-density ionizing radiation

Sabrina Pobiega<sup>1</sup>, Olivier Alibert<sup>2</sup> and Stéphane Marcand<sup>1,\*</sup>

<sup>1</sup>Université de Paris and Université Paris-Saclay, Inserm, CEA IBFJ/iRCM, UMR Stabilité Génétique Cellules Souches et Radiations, 92265 Fontenay-au-Roses, France and <sup>2</sup>Université Paris-Saclay, CEA IBFJ/CNRGH, 91057 Evry, France

Received November 23, 2020; Revised March 31, 2021; Editorial Decision May 22, 2021; Accepted May 27, 2021

## ABSTRACT

**Chromosome fusions threaten genome integrity and promote cancer by engaging catastrophic mutational processes, namely chromosome breakage–fusion–bridge cycles and chromothripsis. Chromosome fusions are frequent in cells incurring telomere dysfunctions or those exposed to DNA breakage. Their occurrence and therefore their contribution to genome instability in unchallenged cells is unknown. To address this issue, we constructed a genetic assay able to capture and quantify rare chromosome fusions in budding yeast. This chromosome fusion capture (CFC) assay relies on the controlled inactivation of one centromere to rescue unstable dicentric chromosome fusions. It is sensitive enough to quantify the basal rate of end-to-end chromosome fusions occurring in wild-type cells. These fusions depend on canonical nonhomologous end joining (NHEJ). Our results show that chromosome end protection results from a trade-off at telomeres between positive effectors (Rif2, Sir4, telomerase) and a negative effector partially antagonizing them (Rif1). The CFC assay also captures NHEJ-dependent chromosome fusions induced by ionizing radiation. It provides evidence for chromosomal rearrangements stemming from a single photon–matter interaction.**

## INTRODUCTION

Chromosome stability requires that DNA double-strand breaks (DSBs) are repaired by canonical nonhomologous end joining (NHEJ) or homologous recombination. NHEJ is an efficient pathway directly resealing DSB ends, most often accurately (1–3). In line with other DNA repair pathways, NHEJ repair sometimes comes with errors. Its contribution to mutagenesis is 2-fold: sequence changes at the

break sites and chromosomal rearrangements (1–9). NHEJ-dependent chromosomal rearrangements include dicentric chromosomes that lead to catastrophic mutational processes, namely chromosome breakage–fusion–bridge cycles and chromothripsis (10–12). The rarity of these events is key to genome integrity.

NHEJ's Achilles heel is its susceptibility to the co-occurrence within the cell nucleus of multiple DSBs, a situation that ionizing radiation easily creates (13–16). This co-occurrence favours DNA end erroneous resealing stemming from distinct breaks, resulting in chromosome translocations. NHEJ error frequency results from a balance between broken end diffusion and their synapsis (tethering) by the NHEJ machinery (4,8,17,18).

An efficient NHEJ machinery must also co-exist in the nucleus with stable telomeres, the native chromosome ends. This restriction to DSB is an important element of NHEJ accuracy. It is based on a strong inhibition of NHEJ at telomere ends, which ensures that chromosome ends rarely fuse. NHEJ inhibition relies on a limited number of proteins present at telomeres. Defects in these proteins or telomere shortening, which reduce their amount, compromise NHEJ inhibition and lead to frequent chromosome fusions (11,19–23). Chromosome fusions may occur in unchallenged cells, but due to technical limitations their frequency and therefore the absolute efficiency of NHEJ inhibition at functional telomeres remains difficult to assess.

The rate of telomere fusions has been explored in the *Schizosaccharomyces pombe* and *Saccharomyces cerevisiae* yeast model organisms. In fission yeast, a genetic assay capturing fusions between the telomeres of a plasmid-based mini-chromosome shows that telomeres in unperturbed wild-type cells may be more prone to NHEJ-dependent fusions than initially thought ( $\sim 10^{-4}$  events per cell), with the caveat that mini-chromosome telomeres may not be fully functional (24). In budding yeast, a genetic assay capturing NHEJ-dependent fusions between an endonuclease-induced broken end and native telomeres shows that these types of events are rare in wild-type cells, with a frequency

\*To whom correspondence should be addressed. Tel: +33 1 46 54 82 33; Email: [stephane.marcand@cea.fr](mailto:stephane.marcand@cea.fr)

of around  $10^{-7}$  fusions per cell (25). This sensitive assay misses the fusions between native telomeres. PCR-based assays that detect the frequent NHEJ-dependent fusions occurring between dysfunctional telomeres in mutant contexts fail to capture the rarer fusions that may occur in wild-type cells (26–31). The detection threshold of these PCR-based assays is  $\sim 10^{-5}$  to  $10^{-6}$  fusions per cell. Therefore, a quantitative knowledge of telomere fusion contribution to genome instability in normal cells is still missing.

This led us to construct a genetic assay able to capture and quantify rare chromosome fusions in *S. cerevisiae*. This assay relies on the controlled inactivation of one centromere to rescue unstable dicentric chromosome fusions. Sensitive enough to explore wild-type contexts, it shows the rarity of telomere fusions in wild-type yeast cells ( $< 10^{-6}$  events per cell) and the synergy of the pathways inhibiting NHEJ at telomeres. Telomere length is also a key determinant of telomere protection efficiency since telomerase loss causes a rapid increase in fusion frequency. Unexpectedly, this new assay also captures NHEJ-dependent chromosome fusions induced by ionizing radiation. Our data suggest that a single photon–matter interaction can be sufficient to generate an NHEJ-dependent rearrangement.

## MATERIALS AND METHODS

### Chromosome fusion capture and analysis

Strains, plasmids and primers used in this study are listed in Supplementary Table S1. Telomeres and telomere fusions were amplified as previously described using primers TEL6R#31, X2, Y'2 and polyG14 (29,30,32).

To determine survival to *CEN6* loss, cells grown on rich glucose medium (YPD) plates are picked and plated on glucose medium plates lacking uracil to counterselect rare cells having already lost *CEN6* due to Cre background expression in the absence of galactose. After 24 h of growth at 30°C, distinct re-streaks are used to inoculate distinct liquid cultures in YPD. Each culture is then grown to saturation for 3 days at 30°C prior to plating on a galactose medium plate lacking leucine ( $5 \times 10^7$  cells per plate or less if the frequency of survival to *CEN6* loss is above  $4 \times 10^{-6}$ ). Colonies are counted after 5–7 days at 30°C. Each data point comes from an independent re-streak and an independent cell culture spread on a single plate.

A few strains used here lack the *kILEU2* marker inserted at *CEN6* but possess a second marker (*NAT<sup>r</sup>*) within the loxP cassette. For those strains, cells were plated on galactose complete medium and the grown colonies were replicated on 5-FOA plates to identify clones having lost the *CEN6*-linked *kIURA3* marker. On a sample of survivors (10 per plate), *CEN6* loss was confirmed by assessing the loss of the second *CEN6*-linked marker (*NAT<sup>r</sup>*).

### Sequencing and sequence analysis

Illumina paired-end whole-genome sequencing files were processed with FastQC (v 0.11.4) for quality control and adapter sequences were removed with Cutadapt (v 1.13). Mapping was performed on the reference *S. cerevisiae* genome (assembly sacCer3). Paired ends from chromosome

6 with discordant mapping on the reference genome were identified with samtools (v 1.3.1) and a PERL script was used to align the reads together. Resolution was improved by visual inspection of the alignments on the breakpoint regions.

### Irradiations

Prior to irradiation, dosimetry was performed with two different ionizing chambers as the recommendation of the AAPM's TG-61 and depending on the irradiation configuration (33). We used a cylindrical ionizing chamber 31010 by PTW with a cavity of 0.125 cm<sup>3</sup> calibrated in <sup>137</sup>Cs air kerma free in air with the PTB reference facility number 1904442. This ionizing chamber was also calibrated in air kerma free in air in a range of 100–280 kV X-rays with the PTB reference facility number 1904444. In addition, we used a plane-parallel ionizing chamber with a cavity volume of 0.02 cm<sup>3</sup> calibrated in a range of 15–70 kV X-rays with the PTB reference facility number 1904440.

We performed gamma-ray irradiations with a GSR D1 irradiator from the GSM Company. It is a self-shielded irradiator with four sources of <sup>137</sup>Cs (a total activity of around 180.28 TBq in March 2014). Cell cultures were grown to saturation in YPD (as described above) and placed in six-well plates (1 ml/well; an independent saturated cell culture for each well). Cells were irradiated with an output of 2.6 or 0.0114 Gy/min at room temperature. For dose fractionation experiments, cells were kept in the six-well plates within the exhausted medium at 30°C between irradiations.

We performed X-ray irradiations with a Small Animal Radiation Research Platform. Dosimetry protocol was calibrated to be adjusted to cell irradiation (34). Two configurations were used. The first configuration used 0.8 mm of beryllium, 220 kV and 0.15 mm of copper for the additional filtration. The half-value layer (HVL) was measured at 0.677 mm of copper in order to obtain the spectrum and the effective energy of the photons: 68.5 keV with SpeakCalc and XmuDAT AIEA's software. The size of the field was 12 cm × 12 cm at FSD 35 cm and the dose output in these conditions was 2.7 Gy/min. The second configuration used 0.8 mm beryllium, 40 kV and 1 mm of aluminium for the additional filtration. The HVL was measured at 0.886 mm of aluminium in order to obtain the spectrum and the effective energy of the photons: 20.4 keV with the SpeakCalc and XmuDAT AIAE's software. The size of the field was 15 cm × 11 cm at FSD 34 cm and the dose output in these conditions was 0.83 Gy/min. Due to the shape and the size of the field and to keep the homogeneity of the irradiation, only four wells on the six-well plate were irradiated (34). Cells were irradiated at room temperature as above.

## RESULTS

### A new assay capturing rare NHEJ-dependent chromosome rearrangements

Chromosome fusions create unstable dicentric chromosomes. The inactivation of one centromere is an efficient way to stabilize dicentric chromosomes and to select chromosome fusions (35–37) (Figure 1A). In a previous study,

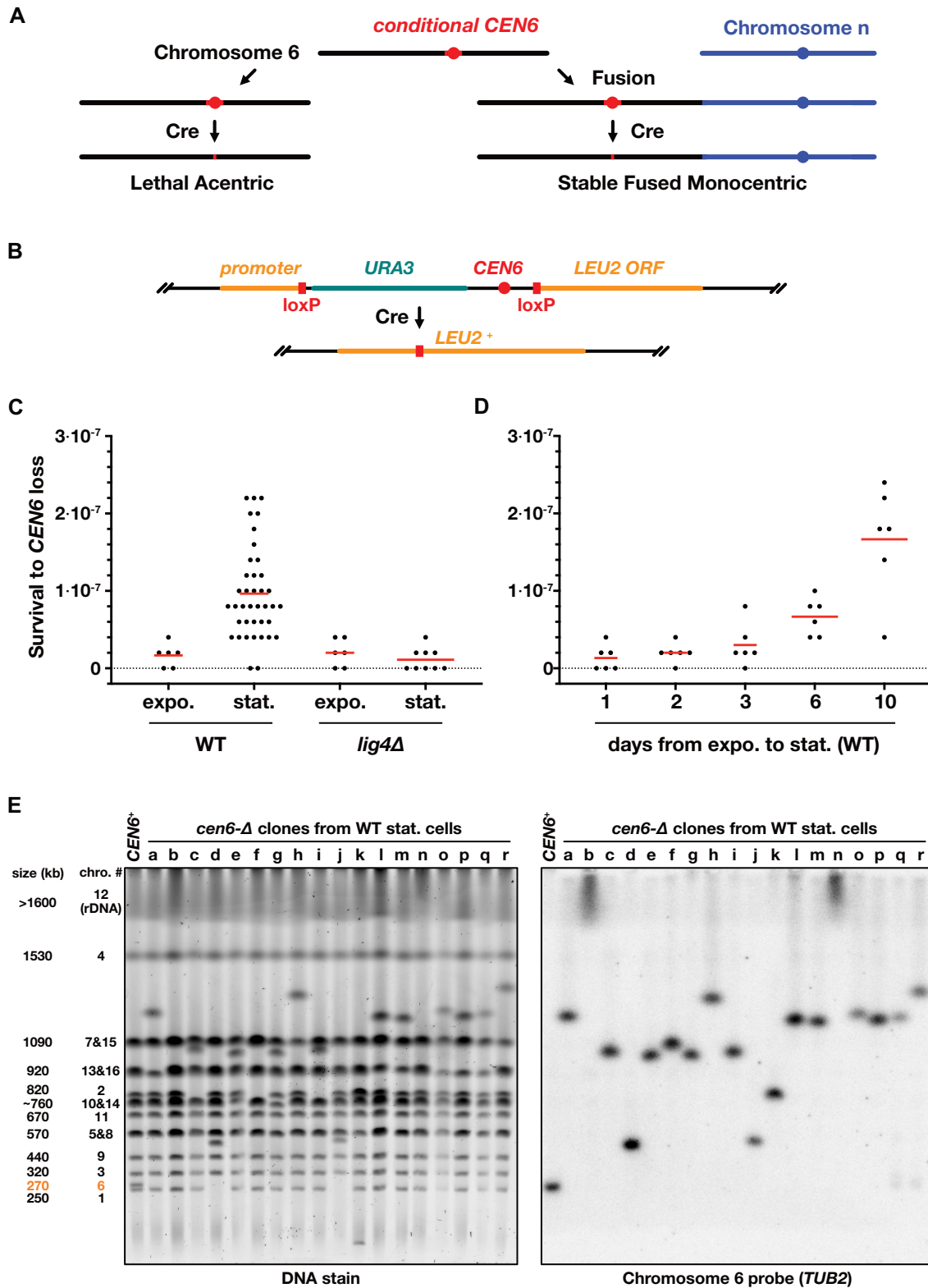


**Figure 1.** An assay to capture chromosome fusions. (A) *CEN6* elimination stabilizes fusions between chromosome 6 and another chromosome. If chromosome 6 is unfused, *CEN6* elimination generates an unstable acentric chromosome leading to cell death. (B) Schematic representation of the loxP cassette inserted at *CEN6*. (C) Survival to *CEN6* loss of wild-type and NHEJ-deficient (*lig4Δ*) cells. Expo.: cells growing exponentially in rich medium ( $OD_{600nm} < 1$ ). Stat.: cells reaching stationary phase in rich medium (3 days,  $OD_{600nm} \approx 25$ ). Each data point from an independent cell culture spread on a single plate. (D) Survival to *CEN6* loss of wild-type cells reaching stationary phase from exponential growth (day 0,  $OD_{600nm} \approx 2$ ). (E) Karyotype of *cen6Δ* clones from wild-type stationary cells. In clones *b* and *n*, chromosome 6 is fused to chromosome 12.

we inactivated the native centromere of *S. cerevisiae* chromosome 6 (*CEN6*) using inducible promoters pointed towards the centromere (36). However, the assay lacks sensitivity to capture fusions in wild-type cells (36). To circumvent this limitation, we created an assay where the Cre recombinase eliminates the centromere. To increase the assay specificity, a promoter and a *LEU2* coding sequence surround a *loxP* cassette that includes *CEN6* and a *URA3* gene (Figure 1B). Cre expression from a galactose-inducible promoter simultaneously deletes *CEN6* and generates a functional *LEU2* gene. The latter allows a counterselection of cells having failed Cre-induced recombination ( $\sim 1$  every  $10^5$  cells) by screening for leucine prototrophic *cen6*- $\Delta$  clones on galactose medium lacking leucine. Note that we chose chromosome 6 because the mis-segregation of this chromosome leads to two unviable cells, increasing the stringency of the assay (36,38).

First, we estimated the frequency of survival to *CEN6* loss in wild-type cells (Figure 1C). Cells growing exponentially (expo.) or having reached stationary phase in 6 days (stat.) in liquid glucose-rich medium were spread on galactose medium plates lacking leucine ( $5 \times 10^7$  cells per plate; each data point from a distinct cell culture; see the 'Materials and Methods' section). Most cells only divide a few times, forming a layer of abortive microcolonies. Viable leucine prototrophic colonies emerge on plates after 4–5 days at 30°C. Loss of the *URA3* gene and PCR on a sample of survivors confirm *CEN6* loss. From exponentially growing cells, the frequency of survivors to *CEN6* loss is low,  $\sim 2 \times 10^{-8}$  events per cell (Figure 1C, 0–2 colonies per plate, close to the practical limit of the assay sensitivity). This frequency increases  $\sim 5$ -fold to  $\sim 10^{-7}$  events per cell when cells have reached stationary phase in 6 days prior to plating (Figure 1C). Increased time in stationary phase increases survival to *CEN6* loss (Figure 1D). This shows that events leading to survival accumulate in stationary cells, either because they stop being counterselected in non-dividing cells or because they form more frequently in those cells or both. The increase in stationary cells also indicates that most selected events form prior to plating and centromere elimination. In contrast, rarer events selected from exponentially growing cells might also be secondary outcomes of centromere elimination (37).

Lig4<sup>Dnl4</sup> is the DNA ligase essential to canonical NHEJ (39). Remarkably, in the absence of Lig4, survival remains low when stationary cells are plated on galactose medium lacking leucine ( $\leq 2 \times 10^{-8}$  events per cell; Figure 1C). This shows that the majority of the events that occur in stationary wild-type cells and lead to survival are products of canonical NHEJ.

To determine the chromosome rearrangements captured by the assay, we analysed by pulse-field gel electrophoresis the karyotype of individual *cen6*- $\Delta$  clones obtained from stationary wild-type cells. Figure 1D shows a representative sample of selected clones. In all clones, chromosome 6 and another chromosome (Figure 1D, left panel) are missing at their native position. In most cases, a single new chromosome appears at a size close to the sum of the two missing chromosomes, as expected for chromosome fusions. The fused chromosome hybridizes with a probe from chromosome 6 left arm (Figure 1D, right panel). Thus,

the assay can capture individual chromosome fusions. In a few clones, two new chromosomes appear, suggestive of a reciprocal translocation (e.g. clone *k* in Figure 1D, the smaller of the rearranged chromosomes likely an acentric in multiple copies). In conclusion, the assay captures rare NHEJ-dependent chromosome fusions occurring in stationary wild-type cells.

### Telomere fusions in wild-type cells

Chromosome fusions can stem from fusions between telomeres or be consecutive to telomere losses or internal breaks. To distinguish between these events, we used a Southern blot approach to first determine which chromosome end of chromosome 6 is fused. The sequence adjacent to the right end telomere of chromosome 6 (*TEL6R*) is unique. As shown in Figure 2A (right panel, same clones as in Figure 1D), instead of the characteristic smear of intact telomeres, some captured chromosome fusions display a discrete-size band, indicating that *TEL6R* is fused (e.g. clones *a*, *l* and *n*), or no signal at *TEL6R* (e.g. clone *d*), indicating that this telomere is lost. Among the 47 clones with a chromosome fusion that were tested at *TEL6R*, 11 are fused at *TEL6R* ( $\sim 23\%$ ) and 3 have lost *TEL6R* ( $\sim 6\%$ ).

The sequence adjacent to the left end of chromosome 6 (*TEL6L*) is one of the *Y'* repeated elements, 5–7 kb sequences present at the end of approximately half of the *S. cerevisiae* telomeres. The first stretch of non-repeated sequences is  $\sim 6$  kb from the chromosome end and we used this sequence as a probe to identify which clones have fused at *TEL6L* (Figure 2A, left panel; *TEL6L* position marked with a blue arrow and other cross-hybridizing restriction fragments marked with asterisks). As expected, the clones with a rearranged *TEL6R* display an intact *TEL6L* (e.g. clones *a*, *d*, *l* and *n*). Among the other clones, some display a new band indicative of a fusion event preserving at least a part of *TEL6L* (e.g. clones *b*, *e*, *f*, *j*, *m*, *p*, *q* and *r*). A shorter restriction fragment indicates that the terminal TG<sub>1-3</sub> telomere sequences from *TEL6L* are lost in the fusion (e.g. clones *e*, *m*, *q* and *r*). Other clones have lost the probed sequence, indicating a more extensive loss of 6L chromosome end (e.g. clones *c*, *g*, *h* and *i*). Clones with an apparent reciprocal translocation maintain both chromosome 6 telomere ends (e.g. clone *k*, whose *TEL6R* end is in multiple copies). Among 47 clones with a chromosome fusion that were tested, 19 are fused at *TEL6L* ( $\sim 40\%$ ) and 14 have lost *TEL6L* ( $\sim 21\%$ ).

Overall, a fraction of the captured chromosome fusions involves the loss of one chromosome 6 telomere ( $\sim 30\%$ ). Are TG<sub>1-3</sub> telomere repeats still present at the fusion point in the remaining clones? Telomeres and subtelomeres are repeated sequences and their head-to-head fusion generates palindromes difficult to amplify and to sequence. Using a primer specific to *TEL6R* and a primer specific to *Y'* element distal end, we could amplify some of the fusions at *TEL6R* (4 out of 11) (Figure 2B). Sequencing shows that three possess TG<sub>1-3</sub> telomere repeats in head-to-head orientation (clones  $\gamma$ ,  $\delta$  and  $\eta$ , the palindromic fusion points could not be sequenced) and one a fusion between a very short *TEL6R* and a truncated tandem of *Y'* elements (clone *n*) (Figure 2B). Together, these results show that a fraction

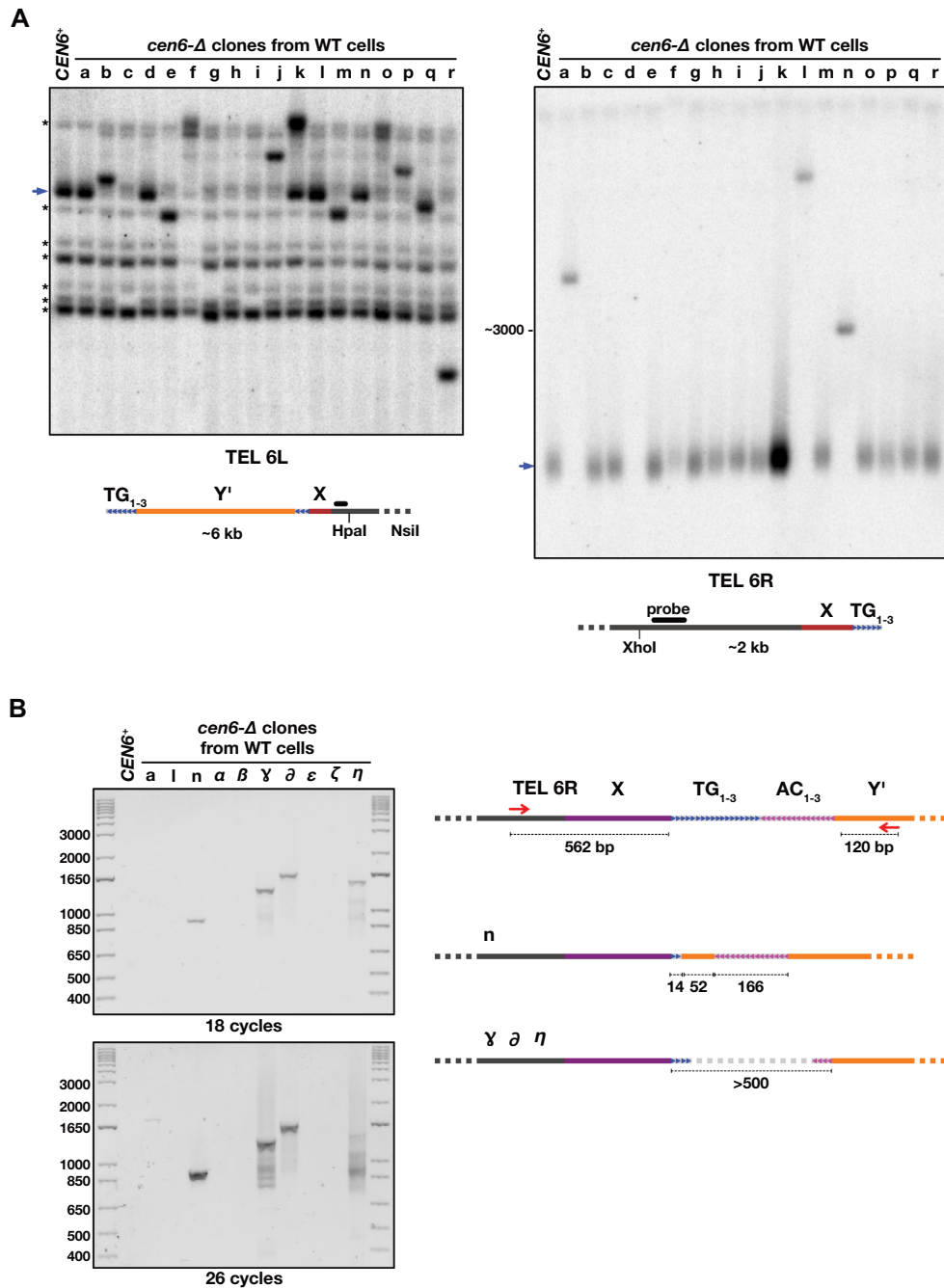


**Figure 2.** Telomere fusions in wild-type cells. (A) Telomere fusions at chromosome 6 telomeres among *cen6*Δ clones from wild-type stationary cells. Same clones as in Figure 1D. *TEL6L* and *TEL6R* positions marked with blue arrows. Cross-hybridizing restriction fragments marked with asterisks. (B) PCR amplification of fusions between chromosome 6 right telomere (*TEL6R*) and Y'-containing telomeres.

of the chromosome fusions captured from unchallenged wild-type cells results from a fusion between two native telomeres.

**NHEJ-dependent chromosome fusions in response to defects in telomere functions**

Next, we asked whether the chromosome fusion capture (CFC) assay can help to better assess the function of individual telomeric factors in chromosome end protec-

tion. In budding yeast, the essential protein Rap1 covers TG<sub>1-3</sub> telomere repeats. Through direct interactions with its C-terminal domain, Rap1 recruits to telomeres other proteins that contribute to telomere functions and telomere length homeostasis. Previous works showed that the Rap1-interacting factors Rif2 and Sir4 act in synergy to prevent NHEJ-dependent telomere–telomere fusions (29–31,40). This conclusion was based on a PCR assay that could only detect relatively high frequencies of telomere fusions, for instance, those occurring in cells lacking both Rif2

and Sir4. The PCR assay failed to assess the impact of single mutants (29–31,40). To address this issue, we tested the individual contribution of these factors to the low frequency of chromosome fusions observed in wild-type cells using the new CFC assay.

As shown in Figure 3A, the loss of Rif2 or Sir4 increases survival to *CEN6* loss ~3- and 30-fold, respectively. This indicates that chromosome fusions are more frequent in these single mutants, in agreement with a previous observation for Rif2 (25). Analysis of individual *cen6-Δ* clones obtained from Rif2 and Sir4 defective cells shows that each clone stems from a single chromosome fusion between chromosome 6 and another chromosome. In contrast to wild-type cells, fusions in cells lacking Rif2 occur at one of the two telomeres of chromosome 6 with similar probabilities (Figure 3B and Supplementary Figure S1A). This suggests that in wild-type cells the Y'-less *TEL6R* telomere relies slightly more on Rif2 than the Y'-containing *TEL6L* telomere. In cells lacking both Rif2 and Sir4, survival to *CEN6* loss further increases to reach a frequency four orders of magnitude above the frequency observed in wild-type cells (Figure 3A). This high survival frequency requires Lig4 indicating that NHEJ produces most of the events leading to survival. Together, these results confirm that Rif2 and Sir4 act in synergy to oppose NHEJ at telomeres. In addition, they show that Rif2 and Sir4 are both essential and non-redundant to bring down NHEJ between telomeres to the very low level observed in normal cells.

We then addressed the impact on telomere protection of two other proteins recruited by Rap1 to telomeres, Rif1 and Sir3 (29). As Rif2, Rif1 represses telomere elongation by telomerase (31,41–46). The absence of Rif1 both elongates telomeres and facilitates the binding of Rif2 and Sir4 to telomeres (41,47,48). In association with Sir4, Sir3 is a core component of yeast heterochromatin and clusters telomeres within the nucleus (49,50). The absence of Sir3 does not elongate telomeres but favours Rif1 and Rif2 binding to Rap1 (48). As shown in Figure 3A, the absence of Rif1 or Sir3 lowers the basal rate of chromosome fusions (~3-fold reduction relative to wild-type cells). Thus, both Rif1 and Sir3 are impediments to telomere protection against NHEJ-dependent fusions in wild-type cells, perhaps by limiting telomere elongation (Rif1; see below), by limiting Rif2 or Sir4 recruitment (Rif1 and Sir3) and by bringing telomere in close proximity (Sir3). These data also confirm that Sir4 functions in telomere protection and heterochromatin are distinct (29).

### NHEJ-dependent chromosome fusions in response to changes in telomere length

Next, we asked how telomere length variations change the frequency of chromosome fusions. A means to increase telomere length in a native context (i.e. with a wild-type proteome) is to transiently grow cells in the presence of ethanol (51,52). To elongate telomeres, we grew wild-type cells for 10 to 20 generations in glucose-containing rich medium complemented with 5% ethanol and then we allowed them to reach stationary phase in glucose-containing rich medium lacking ethanol (for ~5 generations) prior to plating on galactose medium plates lacking leucine. As

shown in Figure 3A, the induced telomere elongation (Supplementary Figure S1B) correlates with a lower survival to *CEN6* loss, suggesting that telomere length is a limiting factor for telomere protection against fusions in wild-type cells.

As an additional means to tune telomere length and explore its impact on chromosome fusion frequency, we used a conditional allele of telomerase, *tetO-tlc1*, in which a doxycycline-repressible promoter controls the gene encoding telomerase ARN template *TLC1<sup>TRT</sup>* (53,54). In uninduced condition (without doxycycline), this allele shortens telomeres (53) (Supplementary Figure S1B) and causes an ~100-fold increase in chromosome fusion frequency (Figure 3A). Telomerase inactivation by doxycycline for 10 and 20 population doublings further decreases telomere length and further increases chromosome fusion frequency ~5- and 15-fold, respectively (~500/1500-fold compared to wild-type cells). Bringing back telomeres towards wild-type length by growing *tetO-tlc1* cells in ethanol (53) brings back chromosome fusion frequency close to the wild-type level, indicating that short telomeres are the cause of the chromosome fusion increase in telomerase-defective cells. Analysis of individual *cen6-Δ* clones from *tetO-tlc1* cells shows that each clone displays a fusion between chromosome 6 and another chromosome. Fusions at *TEL6R* are more frequent in *tetO-tlc1* cells exposed to doxycycline (Figure 3B and Supplementary Figure S2A), suggesting that the Y' element present at *TEL6L* may offer some buffering in response to a transient telomerase deficiency.

The loss of Lig4 reduces chromosome fusion frequencies in telomerase-defective cells by ~20–50-fold, showing that canonical NHEJ is the main source of the events captured by the assay in response to telomerase inactivation. The absence of Lig4 also reveals that telomere shortening leads to increased frequencies of NHEJ-independent events (Figure 3A). We analysed individual *cen6-Δ* clones from *tetO-tlc1 lig4Δ* cells. In a majority of clones, one telomere of chromosome 6 is lost (Supplementary Figure S2B), indicating that Lig4-independent fusions often occurred at more internal positions within the chromosome.

As shown in Figure 3A, Rif1 loss also strongly reduces the frequency of chromosome fusions induced by the *tetO-tlc1* allele, in both uninduced (–dox) and induced (+dox) conditions. This suppression correlates with an increased telomere length in *tetO-tlc1 rif1Δ* cells (Supplementary Figure S1B). Another means to shorten telomeres is to inactivate the Tel1<sup>ATM</sup> kinase, an activator of telomere elongation by telomerase (26,27,55,56). Tel1 loss, which shortens telomere length ~2-fold, leads to a 2000-fold increase in survival to *CEN6* loss (Figure 3A). In cells lacking Tel1, Rif1 loss brings telomere length closer to the wild-type length (Supplementary Figure S1B) and strongly reduces the frequency of chromosome fusions (Figure 3A). Together, these data show that changes in telomere length have large effects on chromosome end protection.

### NHEJ-dependent chromosome fusions induced by ionizing radiation

Since the assay captures NHEJ-dependent chromosome fusions, we next used it to explore NHEJ repair of co-occurring DNA DSBs. To generate random co-occurring

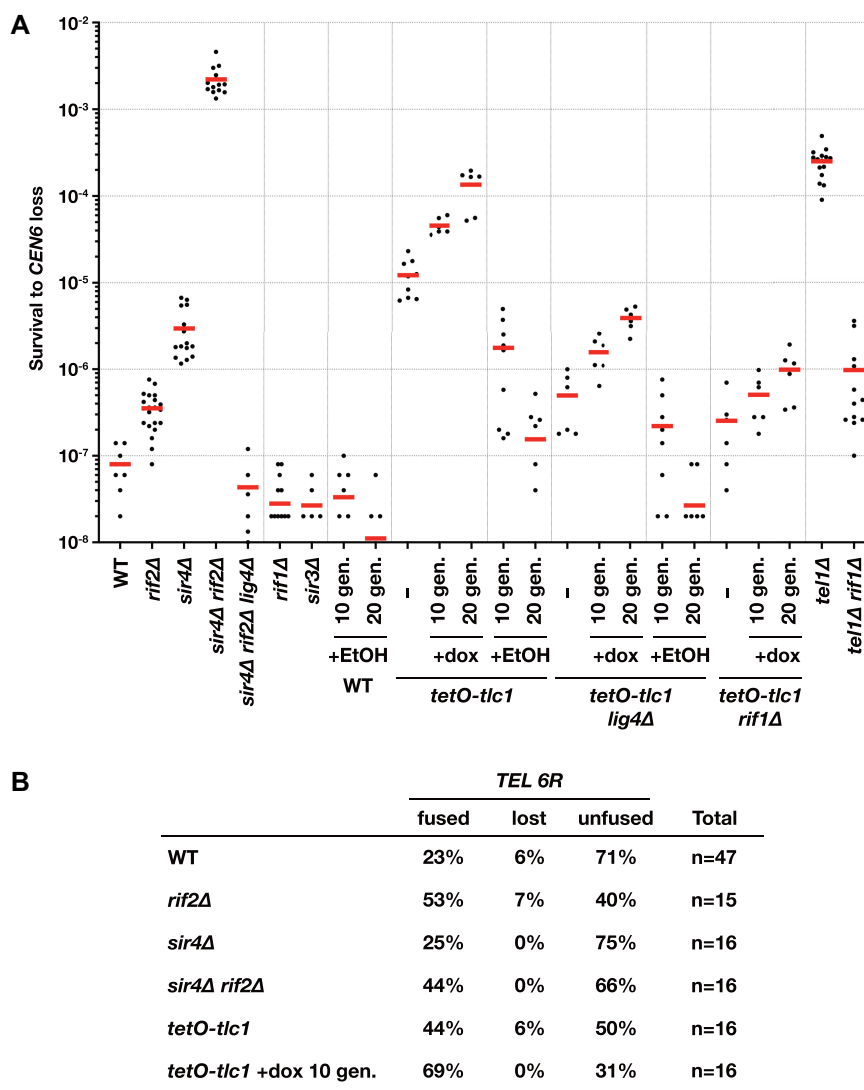


**Figure 3.** NHEJ-dependent chromosome fusions in response to defects in telomere function. (A) Survival frequency to *CEN6* loss in stationary cells lacking Rif2, Sir4, Rif1, Sir3, Tel1 and telomerase template RNA (*TLCI*). +EtOH: growth for 10 or 20 generations in glucose-containing rich medium complemented with 5% ethanol followed ~5 generations in glucose-containing rich medium lacking ethanol to reach stationary phase. +Dox: growth to saturation for 10 or 20 generation in glucose-containing rich medium complemented with 30  $\mu\text{g}/\text{ml}$  doxycycline. Telomere length in stationary phase at the time of plating shown in Supplementary Figure S1B. (B) Telomere fusions at chromosome 6 right telomere among *cen6Δ* clones from wild-type and mutant stationary cells.

DSBs, cells grown to stationary phase in liquid rich medium were irradiated with gamma rays stemming from  $^{137}\text{Cs}$  decay (662 keV, 2.60 Gy/min) prior to plating on galactose medium lacking leucine. As shown in Figure 4A, irradiation leads to an increase in survival to *CEN6* loss that is correlated to the received dose. The observed inflection at 40 Gy can be explained by an overall loss of cell viability at this dose (Figure 4B and Supplementary Figure S3A) (2,57). The increase in survival to *CEN6* loss requires Lig4 (Figure 4A), indicating that canonical NHEJ generates most of the radiation-induced events selected by the assay. Since a single unrepaired DSB would be lethal in haploid cells, the overall cell viability in the absence of Lig4 (Figure 4B) provides a rough estimate of the number of radiation-induced DSBs per cell (e.g. about one or a few DSBs in up to half of cells ex-

posed to 40 Gy). Analysis of individual radiation-induced *cen6Δ* clones from wild-type cells shows that each clone displays a fusion between chromosome 6 and another chromosome, or, more rarely, a reciprocal translocation (Figure 4C).

Contrary to telomere–telomere fusions between chromosome 6 and another chromosome that always lead to viable outcomes once *CEN6* is deleted, we expect that the assay only selects a fraction of the chromosome 6 rearrangements stemming from radiation-induced DSBs. Fusions resulting in the loss of essential genes are not viable in haploid cells and therefore will not be selected. In practice, this severe constraint restricts viable chromosome fusions to those stemming from DSBs occurring within subtelomeric regions, which lack essential genes in yeast. On chro-

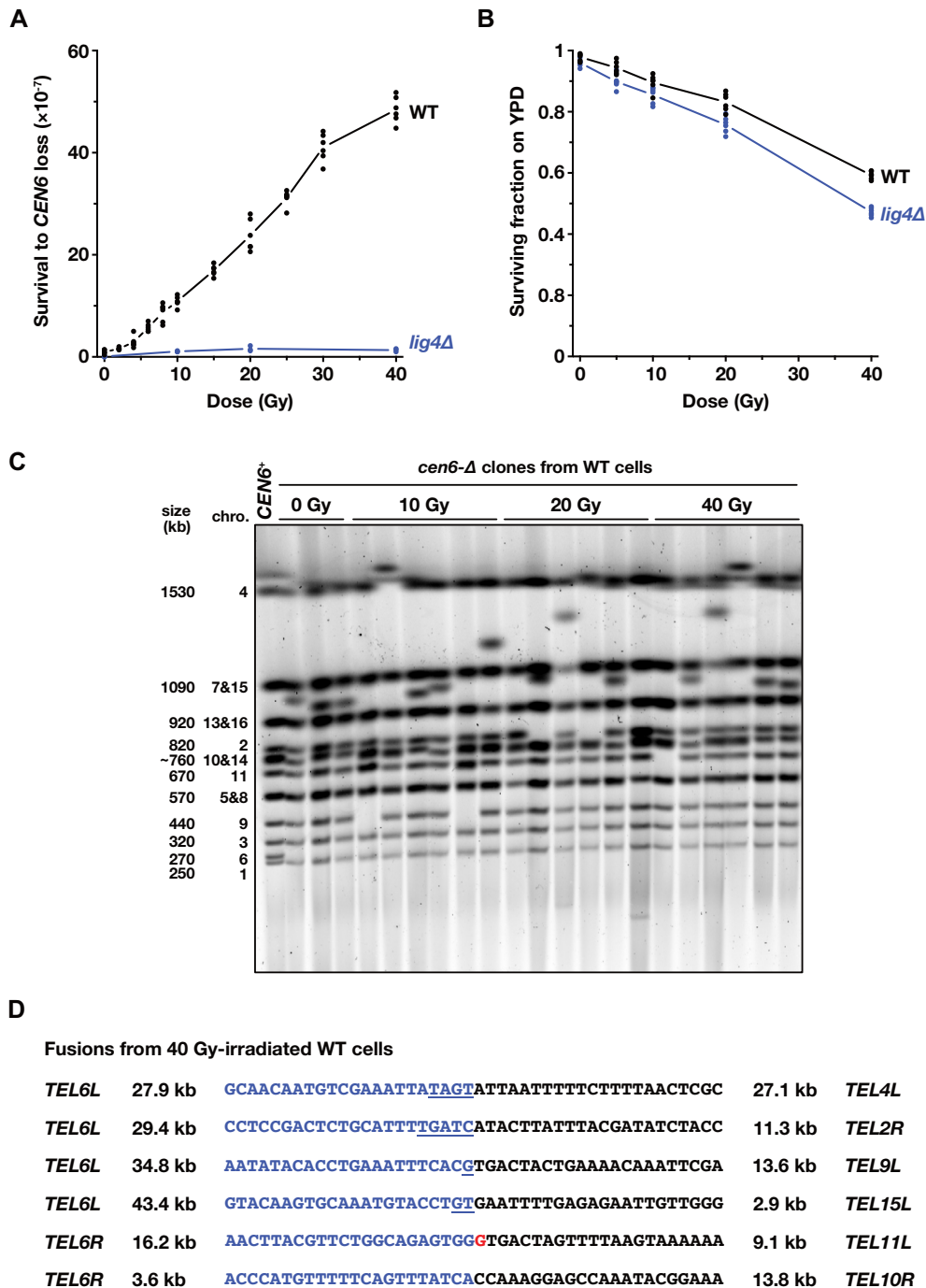


**Figure 4.** NHEJ-dependent chromosome fusions induced by ionizing radiation. (A) Survival to *CEN6* loss in response to gamma-ray irradiation ( $^{137}\text{Cs}$ ). (B) Cell survival in response to gamma-ray irradiation. (C) Karyotype of *cen6* $\Delta$  clones from irradiated wild-type stationary cells. (D) Fusion point sequence in *cen6* $\Delta$  clones from irradiated wild-type stationary cells. Blue: chromosome 6 sequence. Underlined: microhomology at the junction. Red: added non-homologous base. Distance from the closest telomere in kb.

mosome 6, this is 43.6 kb on the left end and 16.7 kb on the right end, representing together  $\sim 0.5\%$  of the genome. On other chromosomes, non-essential subtelomeric regions are  $\sim 30$  kb long and constitute together  $\sim 7.5\%$  of the genome (combinatorial probability  $\sim 0.04\%$ ). In addition, we expect that the assay cannot select reciprocal translocations leading to unstable acentric chromosomes or interrupting essen-

tial genes. To test this prediction, we sequenced the genome of six clones with a radiation-induced chromosome fusion. All display a fusion between non-essential subtelomeric regions (Figure 4D). The fusion points lack extensive homology, as expected for canonical NHEJ products. These data confirm that viability restricts the captured events to a small fraction of the radiation-induced chromosomal re-

arrangements. In agreement with this conclusion, irradiation of NHEJ-proficient diploid cells (with a conditional *CEN6* on both chromosomes 6) leads to a relative increase in survival to *CEN6* loss compared to haploid cells (Supplementary Figure S4). The spatial proximity between subtelomeres may also favour rearrangements between these regions (7,50,58,59). Despite these limitations, the assay offers a new, sensitive and quantitative method to address NHEJ repair of radiation-induced DSBs.

### Impact of dose fractionation over time on the frequency of radiation-induced rearrangements

First, to assess the specificity of radiation-induced rearrangements, we asked whether photons of distinct energy have a similar ability to cause chromosomal rearrangements in haploid cells. In addition to 662 keV gamma rays, we irradiated cells with X-rays of 68.5 and 20.4 keV effective energies, respectively. All three lead to similar frequencies of chromosomal rearrangements (Figure 5A). This result fits with previous observations in human cells and the predicted energies of the ionizing events (60). As expected, UVC irradiation, whose photon energy is too low to generate DSBs, does not lead to an increased survival to *CEN6* loss (Figure 5B).

NHEJ-dependent radiation-induced rearrangements result from the erroneous repair of co-occurring DSBs (15,16,61). This co-occurrence can stem from independent photon–matter interactions, each leading indirectly to the breakage of the two strands of distinct DNA molecules. Since the frequency of co-occurrence of independent events is the product of the probability of each individual event, this scenario predicts that the frequency of radiation-induced rearrangements should be proportional to the square of the received dose and sensitive to dose fractionation over time (which decreases the probability of co-occurrence). Alternatively, two co-occurring DSBs can stem from a single photon–matter interaction leading to the simultaneous breakage of two distinct DNA molecules (i.e. four strands). In this second scenario, the frequency of radiation-induced rearrangements is linked to a single initiating event and should progress linearly with the received dose and be insensitive to dose fractionation over time.

To test the relevance of these scenarios in our assay, cells in stationary phase were irradiated either once with a full dose or twice with half-doses separated by a 24-h interval at 30°C. As shown in Figure 5C, fractionating a dose of 10 Gy (662 keV gamma rays) significantly reduces the frequency of captured rearrangements by ~30%. At lower doses, the impact of a 24-h dose fractionation progressively lessens to disappear with an irradiation of 4 Gy. In addition, dose fractionation brings the frequency of the induced events closer to a linear (additive) increase with the dose (Supplementary Figure S3B). To further assess the impact of dose fractionation over time, we exposed cells in stationary phase to doses of 5 and 10 Gy fractionated four times with a 24-h interval between irradiations. Dose fractionation lowers the frequency of rearrangements induced by 10 Gy but does not significantly impact the frequency of events induced by a lower dose of 5 Gy (Figure 5D). These results fit with a pre-

dominance of radiation-induced chromosomal rearrangements stemming from a single photon–matter interaction at lower doses (5 Gy or less). At higher doses (above 5 Gy), the rearrangements stemming from multiple independent photon–matter interactions likely predominate, explaining their sensitivity to fractionation over time.

In the previous experiment, 24 h separate the irradiations. Next, we asked whether shorter intervals also decrease the frequency of rearrangements induced by a total dose of 10 Gy. As shown in Figure 6A, reducing the time between irradiations reduces the impact of dose fractionation. Consistent with this finding, a 10 Gy irradiation delivered over 14.5 h at a low dose rate of 0.0114 Gy/min generates less rearrangements than a 10 Gy irradiation delivered in a few minutes at a dose rate of 2.6 Gy/min (Figure 6B). These data suggest that DSBs created by the first irradiation remain capable of rearranging with DSBs created by the second irradiation for less than a few hours, consistent with the timescale of DNA repair by NHEJ. Once this delay has passed, chromosomal rearrangements induced by the second irradiation would only add up to the rearrangements induced by the first irradiation. Alternatively, the lowering of rearrangement frequency in response to dose fractionation can be a consequence of changes induced by the first irradiation, perhaps partially buffering cells against subsequent radiation-induced DNA damages? To assess the likelihood of this hypothesis, we tested the impact of a 10 Gy irradiation on cells previously exposed to 5 Gy (2.79 Gy/min, 24 h between the two irradiations). As shown in Figure 6C, an initial 5 Gy irradiation does not lessen the frequency of rearrangements generated by a second irradiation of 10 Gy. This result suggests that yeast cells in stationary phase do not adapt to ionizing radiation, at least for 24 h and regarding the occurrence of radiation-induced DSBs and their repair by NHEJ.

At lower doses (5 Gy or less), chromosomal rearrangements stemming from a single photon–matter interaction can explain the insensitivity to dose fractionation over time. One scenario is that one gamma ray sometimes causes indirectly the breakage of four DNA strands leading to two simultaneous DSBs. On the other hand, rearrangements at lower doses may occur between radiation-induced DSBs and double-strand ends of other origins. NHEJ-deficient haploid cells remain mostly viable in stationary phase (28,57) (Figure 4B), indicating that spontaneous DSBs of endogenous origin are rare events in these cells. DSB competence for NHEJ repair may also be short-lived, making them an unlikely source of ligatable double-strand ends. Another source could be telomere ends. If telomeres could sometimes fuse with radiation-induced DSB ends, telomere–DSB fusions should be frequent and change in telomere protection efficiency should change the frequency of radiation-induced chromosomal rearrangements. To test these predictions, we analysed individual *cen6-Δ* clones from wild-type cells exposed to 5 Gy. In each clone where the right end of chromosome 6 is fused, the telomere is lost but not fused ( $n = 7$ ; Supplementary Figure S5). We also irradiated stationary cells lacking *Rif1* and *Rif2*. *Rif1* loss, which reinforces telomere protection (Figure 3A), has no impact on the occurrence of radiation-induced rearrangements (Figure 6D). As observed above (Figure 3), *Rif2* loss

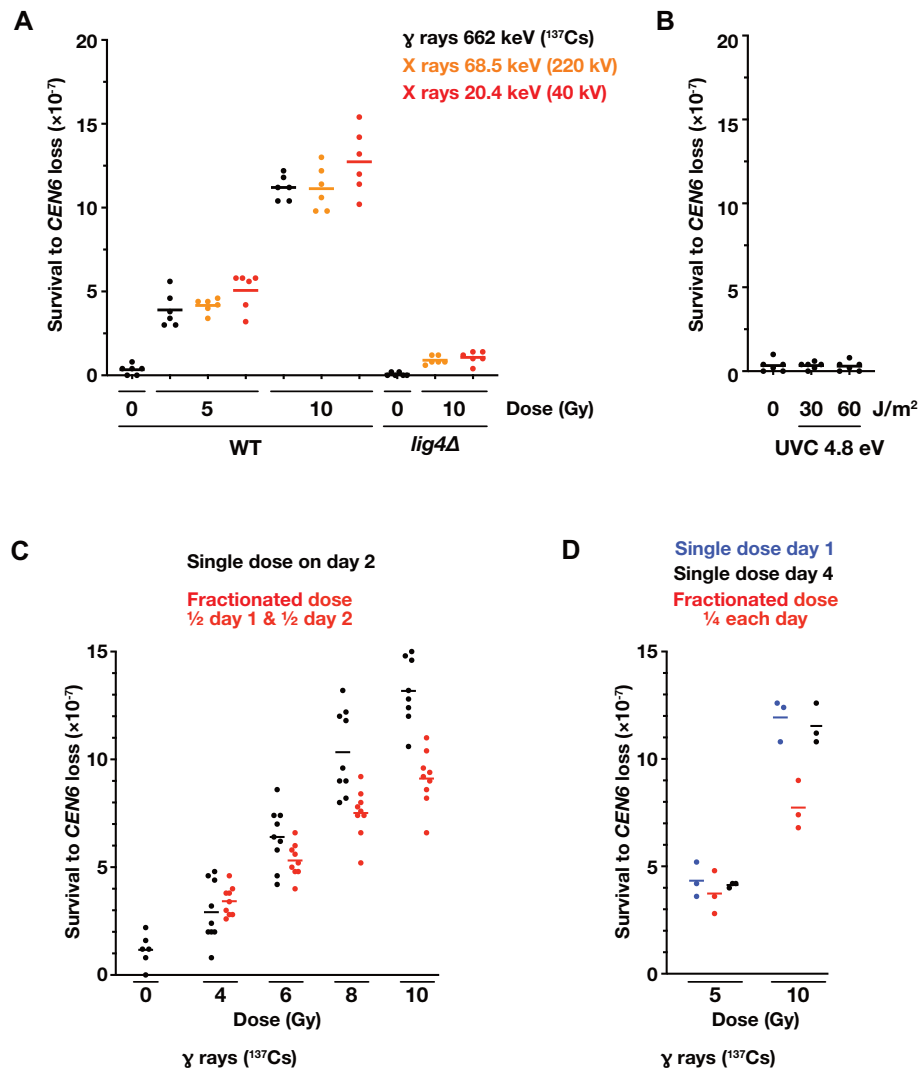


**Figure 5.** Impact of photon energy and dose fractionation on the frequency of radiation-induced rearrangements. (A) Survival to *CEN6* loss in response to X-ray irradiations. (B) Survival to *CEN6* loss in response to UVC irradiations. (C) Survival to *CEN6* loss in response to dose fractionation; 24-h interval and incubation at 30°C between the two half-dose irradiations ( $^{137}\text{Cs}$ ). (D) Dose fractionated four times; 24-h interval and incubation at 30°C between the quarter-dose irradiations ( $^{137}\text{Cs}$ ).

alone partially exposes telomeres to NHEJ, increasing the frequency of chromosome fusions. The rearrangements induced by a 5 Gy irradiation only add up to these events (Figure 6D), indicating that Rif2 loss and ionizing radiation act independently of each other. These results indicate that chromosomal rearrangements induced by 5 Gy do not usually occur between radiation-induced DSBs and telomeres. The more likely scenario is therefore that they are the erroneous repair products of two DSBs whose origin stems from a single photon–matter interaction.

## DISCUSSION

In this work, we developed an assay to capture rare chromosome fusions. This tool shows telomere protection efficiency and measures the contribution of telomere dysfunction to genome instability in unchallenged normal cells. We found that telomere protection requires every pathway

inhibiting NHEJ at telomeres and full telomerase activity. This new assay also captures chromosome rearrangements induced by ionizing radiation and offers evidence for NHEJ-dependent chromosomal rearrangements stemming from single photon–matter interactions.

## Complementarity with the GCR assay

The CFC assay presented here complements the widely used gross chromosomal rearrangement (GCR) assay developed by Kolodner and colleagues (62–64). The latter detects rare losses of a chromosome fragment. Events selected by the GCR assay involve telomere addition at broken ends, interstitial deletions and chromosomal translocations. They rely mostly on error-prone mechanisms such as telomere *de novo* formation, microhomology-mediated end joining and break-induced replication. They still occur in NHEJ-deficient cells. In contrast, the CFC assay mostly captures

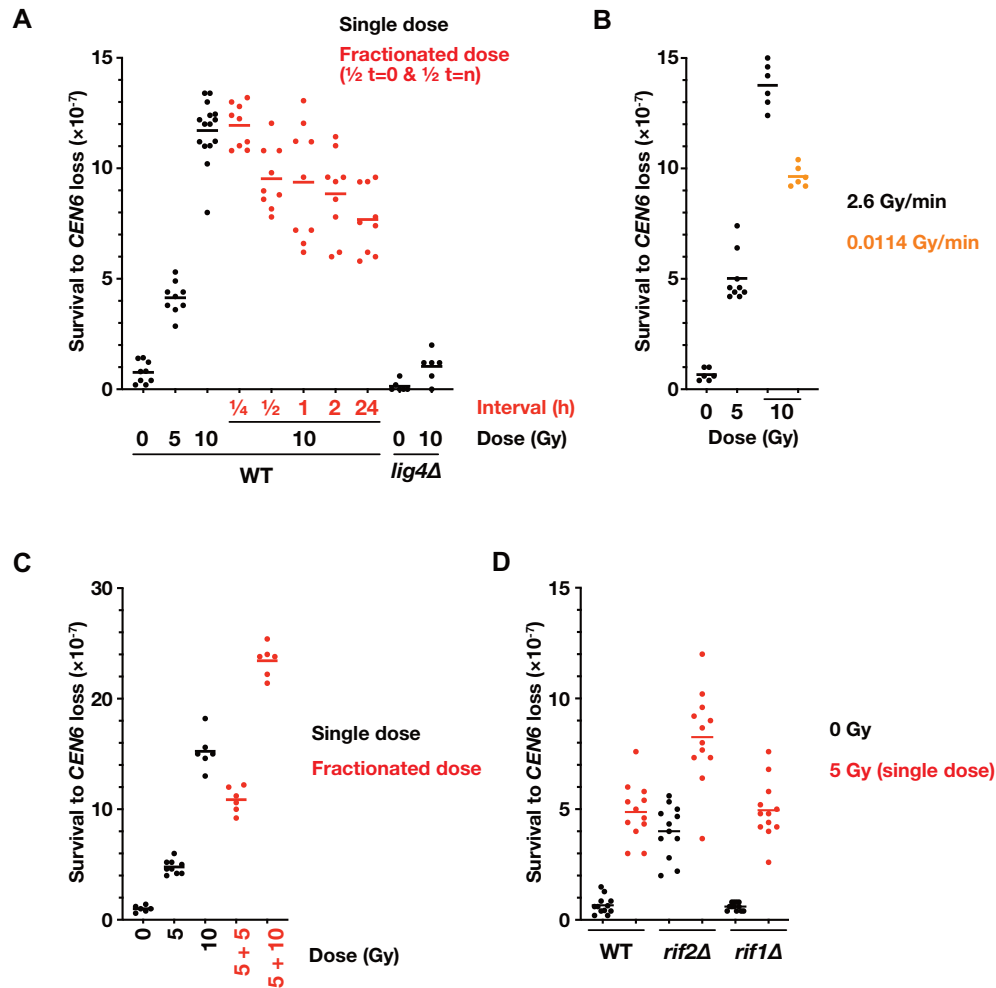


**Figure 6.** Impact of radiation density and telomere protection on the frequency of radiation-induced rearrangements. (A) Impact of the time between two irradiations of 5 Gy ( $^{137}\text{Cs}$ ). (B) Impact of a lower dose rate ( $^{137}\text{Cs}$ ). (C) Impact of a first irradiation on the response to a second irradiation; 24-h interval and incubation at 30°C between the two irradiations ( $^{137}\text{Cs}$ ). (D) Impact of Rif2 and Rif1 loss ( $^{137}\text{Cs}$ ).

events produced by the canonical Lig4-dependent NHEJ pathway. By giving us access to these events, it fills an important gap in the panel of tools available to study genome instability. The assay is amenable to systematic approaches and to genetic screens [e.g. (31)]. In this work, we used it to address the efficiency of NHEJ inhibition at telomeres and the origin of the chromosomal rearrangements induced by ionizing radiation.

### Low frequency of telomere fusions in wild-type cells

The CFC assay provides a first quantification of the basal rate of chromosome fusions occurring in unchallenged wild-type cells. In haploid *S. cerevisiae* cells reaching stationary phase, chromosome 6 is fused to another chromosome in  $\sim 1$  every  $10^7$  cells. With the assumption that all chromosomes are similar in this matter, the frequency of chromosome fusions would be  $\sim 10^{-6}$  per cell. Among the isolated fusions, we found a large fraction of telomere fusions. This indicates that telomere dysfunction in wild-type cells is a significant contributor to the basal level of chromosome fusions, and therefore to time-dependent mutagenesis in quiescence (65–67). Note that in budding yeast, an ad-

ditional rescue pathway reverts telomere fusions into normal telomeres (36,68,69), limiting the impact of telomere fusions on genome stability.

The low frequency of telomere fusions observed in wild-type cells is the end product of the non-redundant actions of Rap1 and its two cofactors Rif2 and Sir4. The CFC assay shows that Rif2 and Sir4 cannot fully back up each other, explaining that both pathways are evolutionarily stable. Efficient telomere protection also requires wild-type telomere length distribution since transient telomerase loss increases the frequency of fusions promptly. The absence of lag in the consequences of telomerase loss might be a hallmark of organisms like yeasts where telomeres are naturally short and telomerase constitutively expressed in all cells. In contrast, the absence of Rif1 diminishes the frequency of telomere fusions. This is a likely consequence of increased telomere length (and therefore increased Rap1 binding) and of reduced competition for Rif2 and Sir4 binding on Rap1. Then, what could be the evolutionary advantage of maintaining Rif1 at telomeres? Rif1 favours telomere stability during replication (42,43,70,71) and this positive function may simply offset Rif1 negative impact on telomere protection against NHEJ.

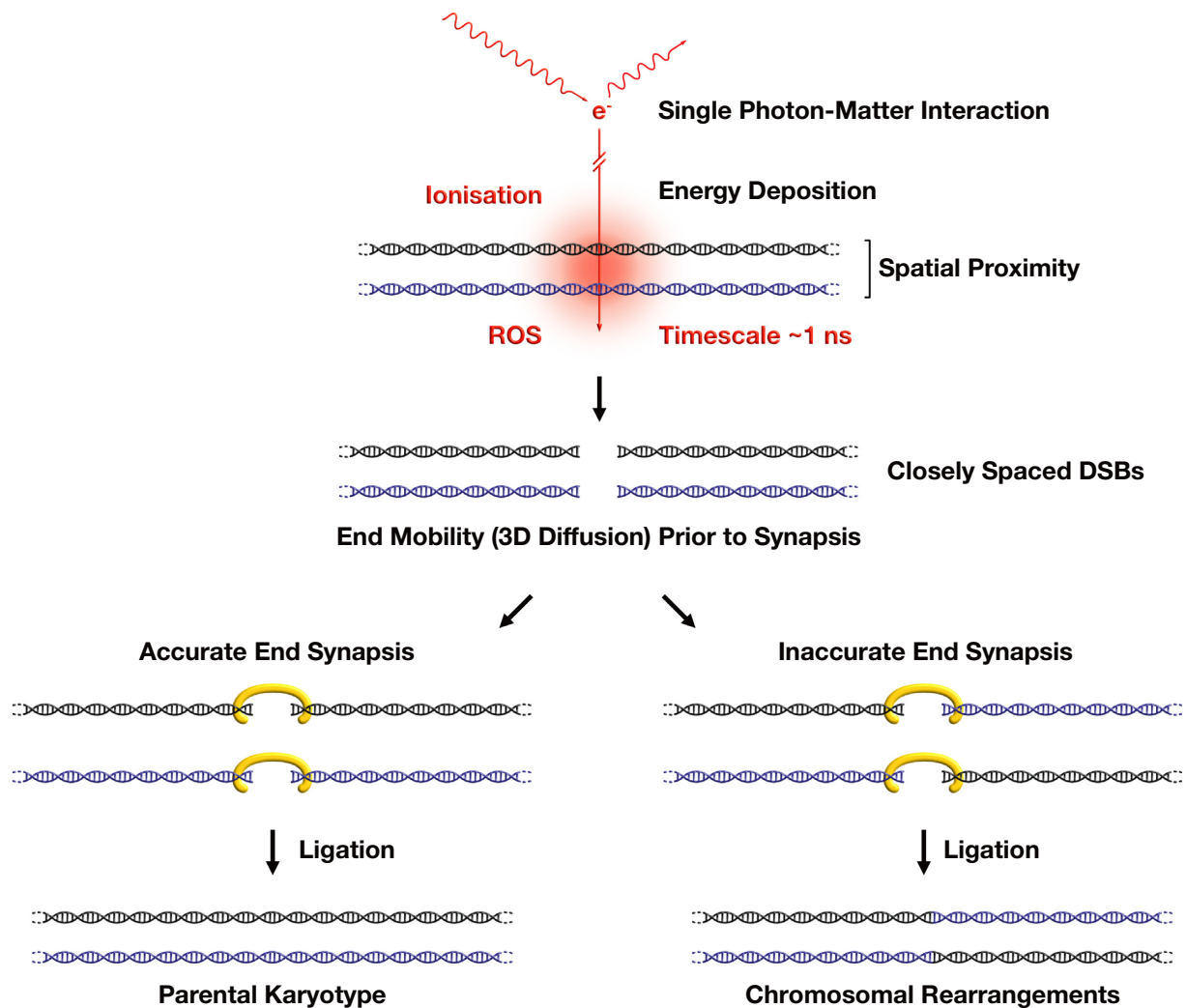


**Figure 7.** Model for NHEJ-dependent chromosomal rearrangements induced by single photon-matter interaction. Localized ionization and ROS formation lead to two closely spaced DSBs and consequently frequent inaccurate end synapsis and repair by NHEJ.

### Evidence for NHEJ-dependent chromosomal rearrangements induced by single photon-matter interaction

The CFC assay provides a new way to quantify radiation-induced NHEJ-dependent chromosomal rearrangements. Its detection threshold is remarkably low, a few Gy. These are very low doses of ionizing radiation for a small-genome organism such as budding yeast [ $1.4 \times 10^7$  bp in a  $2\text{--}3 \mu\text{m}^3$  nucleus (72)]. CFC high sensitivity exposes radiation-induced chromosome fusions whose generation is linear (additive) with the dose and insensitive to radiation intensity. These events predominate at lower doses ( $\leq 5$  Gy) and at lower dose rates ( $\leq 1$  Gy/h). Their linearity and insensitivity to intensity suggest that they stem from one photon-matter interaction (61). Since each of these rearrangements emanates from the repair of two DSBs, this argues that a single photon can lead to two DSBs.

Figure 7 illustrates the molecular steps of this model. An incident gamma photon transfers a fraction of its energy to an electron as kinetic energy. Along its path through matter, the electron deposits this energy through multiple ion-

ization events (including the generation of secondary ionizing electrons). Each energy deposition event can damage DNA directly but also indirectly by creating a transient and local high concentration of reactive oxygen species (ROS) (16,73,74). If this small but highly reactive environment includes two DNA molecules in close proximity, a cluster of four single-strand breaks may form, leading to two coincident DSBs. The four double-strand ends remain mobile relative to each other until they are captured by the NHEJ machinery whose first step is end synapsis (tethering) (8,75). Breakage simultaneity, end proximity and rapid short-distance end diffusion result in frequent inaccurate synapsis (up to a two-third probability if pairing is random) and therefore inaccurate repair. In this model, chromosomal rearrangements are the products of rare but extremely mutagenic events, i.e. the breakage of two adjacent DNA molecules by a single track. An alternative model is that DSBs are produced in distinct energy deposition clusters along the electron path and would usually be distant at the time of their formation. This distance could favour accurate end synapsis and consequently accurate repair by NHEJ. It

may therefore contribute less to mutagenesis. The relative likelihood of the two sequences of events remains to be determined.

The distinctive features of chromosomal rearrangements produced by single photon–matter interaction would be their linear (additive) increase with the dose and their insensitivity to radiation intensity. Exposure of mice to low dose rates of ionizing radiation causes an accumulation of chromosomal rearrangements that is remarkably linear with the dose (76,77), in agreement with pioneering observations on plant cells (61). This suggests that the underlying mechanisms at the origin of these rearrangements are likely conserved in evolution from yeast to mammals. The CFC assay and the mechanism we propose provide a basis to address this issue at a molecular level. It will help to better assess the long-term impact of low-density irradiation and therefore the risks associated with medical radiography and the use of nuclear energy. In addition, the CFC assay can be a simple and sensitive tool to explore the significance of other putative causes of genome instability.

## DATA AVAILABILITY

All relevant data are available from the authors without restriction.

## SUPPLEMENTARY DATA

Supplementary Data are available at NAR Online.

## ACKNOWLEDGEMENTS

We thank Véronique Ménard for irradiation dosimetry, Didier Busso and Eléa Dizet (CIGEX platform) for plasmids, Clémentine Brocas and the CNRGH Sequencing Facility for whole-genome sequencing, and Karine Dubrana, Stefano Mattarocci, Florian Roisné-Hamelin, Zhou Xu, Claude Gazin, Gilles Fisher, Laurent Maloisel, Pablo Radicella, Paul-Henri Roméo, Gaëtan Gruel, Carmen Villagrasa, Nicolas Tang, Laure Sabatier and Christophe Carles for fruitful discussions and suggestions.

## FUNDING

Agence Nationale de la Recherche [ANR-14-CE10-021 DI-CENS, ANR-15-CE12-0007 DNA-Life]; Fondation ARC pour la Recherche sur le Cancer; Commissariat à l'Énergie Atomique et aux Énergies Alternatives (CEA); Electricité de France. Funding for open access charge: CEA.

*Conflict of interest statement.* None declared.

## REFERENCES

- Bétermier, M., Bertrand, P. and Lopez, B.S. (2014) Is non-homologous end-joining really an inherently error-prone process? *PLoS Genet.*, **10**, e1004086.
- Gao, S., Honey, S., Fitcher, B. and Grollman, A.P. (2016) The non-homologous end-joining pathway of *S. cerevisiae* works effectively in G1-phase cells, and religates cognate ends correctly and non-randomly. *DNA Repair (Amst.)*, **42**, 1–10.
- Stinson, B.M., Moreno, A.T., Walter, J.C. and Loparo, J.J. (2020) A mechanism to minimize errors during non-homologous end joining. *Mol. Cell*, **77**, 1080–1091.
- Lee, K., Zhang, Y. and Lee, S.E. (2008) *Saccharomyces cerevisiae* ATM orthologue suppresses break-induced chromosome translocations. *Nature*, **454**, 543–546.
- Gordon, J.L., Byrne, K.P. and Wolfe, K.H. (2011) Mechanisms of chromosome number evolution in yeast. *PLoS Genet.*, **7**, e1002190.
- Yu, Y., Pham, N., Xia, B., Papusha, A., Wang, G., Yan, Z., Peng, G., Chen, K. and Ira, G. (2018) Dna2 nuclease deficiency results in large and complex DNA insertions at chromosomal breaks. *Nature*, **564**, 287–290.
- Sunder, S. and Wilson, T.E. (2019) Frequency of DNA end joining *in trans* is not determined by the predamage spatial proximity of double-strand breaks in yeast. *Proc. Natl Acad. Sci. U.S.A.*, **116**, 9481–9490.
- Wilson, T.E. and Sunder, S. (2020) Double-strand breaks in motion: implications for chromosomal rearrangement. *Curr. Genet.*, **66**, 1–6.
- Shibata, A. and Jeggo, P.A. (2020) Canonical DNA non-homologous end-joining: capacity versus fidelity. *Br. J. Radiol.*, **93**, 20190966.
- Watkins, T.B.K., Lim, E.L., Petkovic, M., Elizalde, S., Birkbak, N.J., Wilson, G.A., Moore, D.A., Grönroos, E., Rowan, A., Dewhurst, S.M. *et al.* (2020) Pervasive chromosomal instability and karyotype order in tumour evolution. *Nature*, **587**, 126–132.
- Umbreit, N.T., Zhang, C.-Z., Lynch, L.D., Blaine, L.J., Cheng, A.M., Tourdot, R., Sun, L., Almubarak, H.F., Judge, K., Mitchell, T.J. *et al.* (2020) Mechanisms generating cancer genome complexity from a single cell division error. *Science*, **368**, eaba0712.
- Maciejowski, J., Chatziplis, A., Dananberg, A., Chu, K., Toufektchan, E., Klimczak, L.J., Gordenin, D.A., Campbell, P.J. and de Lange, T. (2020) APOBEC3-dependent kataegis and TREX1-driven chromothripsis during telomere crisis. *Nat. Genet.*, **52**, 884–890.
- M'kacher, R., Maalouf, E.E.L., Ricoul, M., Heidingsfelder, L., Laplagne, E., Cuceu, C., Hempel, W.M., Colicchio, B., Dieterlen, A. and Sabatier, L. (2014) New tool for biological dosimetry: reevaluation and automation of the gold standard method following telomere and centromere staining. *Mutat. Res.*, **770**, 45–53.
- Abe, Y., Miura, T., Yoshida, M.A., Ujiie, R., Kurosu, Y., Kato, N., Katafuchi, A., Tsuyama, N., Kawamura, F., Ohba, T. *et al.* (2016) Analysis of chromosome translocation frequency after a single CT scan in adults. *J. Radiat. Res.*, **57**, 220–226.
- McMahon, S.J. and Prise, K.M. (2019) Mechanistic modelling of radiation responses. *Cancers (Basel)*, **11**, 205.
- Nickoloff, J.A., Sharma, N. and Taylor, L. (2020) Clustered DNA double-strand breaks: biological effects and relevance to cancer radiotherapy. *Genes (Basel)*, **11**, 99.
- Cajiao, J.J.T., Pietro Carante, M., Rodriguez, M.A.B. and Ballarini, F. (2017) Proximity effects in chromosome aberration induction by low-LET ionizing radiation. *DNA Repair (Amst.)*, **58**, 38–46.
- Shukron, O., Hauer, M. and Holeman, D. (2017) Two loci single particle trajectories analysis: constructing a first passage time statistics of local chromatin exploration. *Sci. Rep.*, **7**, 10346–10311.
- Benarroch-Popivker, D., Pisano, S., Mendez-Bermudez, A., Lototska, L., Kaur, P., Bauwens, S., Djerbi, N., Latrick, C.M., Fraiser, V., Pei, B. *et al.* (2016) TRF2-mediated control of telomere DNA topology as a mechanism for chromosome-end protection. *Mol. Cell*, **61**, 274–286.
- de Lange, T. (2018) Shelterin-mediated telomere protection. *Annu. Rev. Genet.*, **52**, 223–247.
- Van Ly, D., Low, R.R.J., Frölich, S., Bartolec, T.K., Kafer, G.R., Pickett, H.A., Gaus, K. and Cesare, A.J. (2018) Telomere loop dynamics in chromosome end protection. *Mol. Cell*, **71**, 510–525.
- Lototska, L., Yue, J.-X., Li, J., Giraud-Panis, M.-J., Songyang, Z., Royle, N.J., Liti, G., Ye, J., Gilson, E. and Mendez-Bermudez, A. (2020) Human RAPI specifically protects telomeres of senescent cells from DNA damage. *EMBO Rep.*, **2012**, e49076.
- Cleal, K. and Baird, D.M. (2020) Catastrophic endgames: emerging mechanisms of telomere-driven genomic instability. *Trends Genet.*, **36**, 347–359.
- Almeida, H. and Godinho Ferreira, M. (2013) Spontaneous telomere to telomere fusions occur in unperturbed fission yeast cells. *Nucleic Acids Res.*, **41**, 3056–3067.
- DuBois, M.L., Haimberger, Z.W., McIntosh, M.W. and Gottschling, D.E. (2002) A quantitative assay for telomere protection in *Saccharomyces cerevisiae*. *Genetics*, **161**, 995–1013.

26. Chan, S.W.-L. and Blackburn, E.H. (2003) Telomerase and ATM/Tel1p protect telomeres from nonhomologous end joining. *Mol. Cell*, **11**, 1379–1387.
27. Mieczkowski, P.A., Mieczkowska, J.O., Dominska, M. and Petes, T.D. (2003) Genetic regulation of telomere–telomere fusions in the yeast *Saccharomyces cerevisiae*. *Proc. Natl Acad. Sci. U.S.A.*, **100**, 10854–10859.
28. Pardo, B. and Marcand, S. (2005) Rap1 prevents telomere fusions by nonhomologous end joining. *EMBO J.*, **24**, 3117–3127.
29. Marcand, S., Pardo, B., Gratiass, A., Cahun, S. and Callebaut, I. (2008) Multiple pathways inhibit NHEJ at telomeres. *Genes Dev.*, **22**, 1153–1158.
30. Lescasse, R., Pobiega, S., Callebaut, I. and Marcand, S. (2013) End-joining inhibition at telomeres requires the translocase and polySUMO-dependent ubiquitin ligase Uls1. *EMBO J.*, **32**, 805–815.
31. Roisné-Hamelin, F., Pobiega, S., Kévin, J., Miron, S., Depagne, J., Veaute, X., Busso, D., Le Du, M.-H., Callebaut, I., Charbonnier, J.-B. *et al.* (2021) Mechanism of MRX inhibition by Rif2 at telomeres. *Nat. Commun.*, **12**, 2763.
32. Förstemann, K., Höss, M. and Lingner, J. (2000) Telomerase-dependent repeat divergence at the 3' ends of yeast telomeres. *Nucleic Acids Res.*, **28**, 2690–2694.
33. Ma, C.M., Coffey, C.W., DeWerd, L.A., Liu, C., Nath, R., Seltzer, S.M., Seuntjens, J.P. and American Association of Physicists in Medicine (2001) AAPM protocol for 40–300 kV X-ray beam dosimetry in radiotherapy and radiobiology. *Med. Phys.*, **28**, 868–893.
34. Santos Dos, M., Paget, V., Ben Kacem, M., Trompier, F., Benadjaoud, M.A., François, A., Guipaud, O., Benderitter, M. and Milliat, F. (2018) Importance of dosimetry protocol for cell irradiation on a low X-rays facility and consequences for the biological response. *Int. J. Radiat. Biol.*, **94**, 597–606.
35. Ishii, K., Ogiyama, Y., Chikashige, Y., Soejima, S., Masuda, F., Kakuma, T., Hiraoka, Y. and Takahashi, K. (2008) Heterochromatin integrity affects chromosome reorganization after centromere dysfunction. *Science*, **321**, 1088–1091.
36. Pobiega, S. and Marcand, S. (2010) Dicentric breakage at telomere fusions. *Genes Dev.*, **24**, 720–733.
37. Ohno, Y., Ogiyama, Y., Kubota, Y., Kubo, T. and Ishii, K. (2016) Acentric chromosome ends are prone to fusion with functional chromosome ends through a homology-directed rearrangement. *Nucleic Acids Res.*, **44**, 232–244.
38. Torres, E.M., Sokolsky, T., Tucker, C.M., Chan, L.Y., Boselli, M., Dunham, M.J. and Amon, A. (2007) Effects of aneuploidy on cellular physiology and cell division in haploid yeast. *Science*, **317**, 916–924.
39. Chiruvella, K.K., Liang, Z., Birkeland, S.R., Basrur, V. and Wilson, T.E. (2013) *Saccharomyces cerevisiae* DNA ligase IV supports imprecise end joining independently of its catalytic activity. *PLoS Genet.*, **9**, e1003599.
40. Faure, G., Jézéquel, K., Roisné-Hamelin, F., Bitard-Feildel, T., Lamiable, A., Marcand, S. and Callebaut, I. (2019) Discovery and evolution of new domains in yeast heterochromatin factor Sir4 and its partner Esc1. *Genome Biol. Evol.*, **11**, 572–585.
41. Wotton, D. and Shore, D. (1997) A novel Rap1p-interacting factor, Rif2p, cooperates with Rif1p to regulate telomere length in *Saccharomyces cerevisiae*. *Genes Dev.*, **11**, 748–760.
42. Anbalagan, S., Bonetti, D., Lucchini, G. and Longhese, M.P. (2011) Rif1 supports the function of the CST complex in yeast telomere capping. *PLoS Genet.*, **7**, e1002024.
43. Mattarocci, S., Reinert, J.K., Bunker, R.D., Fontana, G.A., Shi, T., Klein, D., Cavadini, S., Faty, M., Shyian, M., Hafner, L. *et al.* (2017) Rif1 maintains telomeres and mediates DNA repair by encasing DNA ends. *Nat. Struct. Mol. Biol.*, **24**, 588–595.
44. Kedziora, S., Gali, V.K., Wilson, R.H.C., Clark, K.R.M., Nieduszynski, C.A., Hiraga, S.-I. and Donaldson, A.D. (2018) Rif1 acts through protein phosphatase 1 but independent of replication timing to suppress telomere extension in budding yeast. *Nucleic Acids Res.*, **46**, 3993–4003.
45. Shubin, C.B. and Greider, C.W. (2020) The role of Rif1 in telomere length regulation is separable from its role in origin firing. *eLife*, **9**, e58066.
46. Fontana, G.A., Hess, D., Reinert, J.K., Mattarocci, S., Falquet, B., Klein, D., Shore, D., Thomä, N.H. and Rass, U. (2019) Rif1 S-acylation mediates DNA double-strand break repair at the inner nuclear membrane. *Nat. Commun.*, **10**, 2535.
47. Buck, S.W. and Shore, D. (1995) Action of a RAP1 carboxy-terminal silencing domain reveals an underlying competition between HMR and telomeres in yeast. *Genes Dev.*, **9**, 370–384.
48. Shi, T., Bunker, R.D., Mattarocci, S., Ribeyre, C., Faty, M., Gut, H., Scrima, A., Rass, U., Rubin, S.M., Shore, D. *et al.* (2013) Rif1 and Rif2 shape telomere function and architecture through multivalent Rap1 interactions. *Cell*, **153**, 1340–1353.
49. Gartenberg, M.R. and Smith, J.S. (2016) The nuts and bolts of transcriptionally silent chromatin in *Saccharomyces cerevisiae*. *Genetics*, **203**, 1563–1599.
50. Ruault, M., Scolari, V.F., Lazar-Stefanita, L., Hoher, A., Loiodice, I., Koszul, R. and Taddei, A. (2021) Sir3 mediates long-range chromosome interactions in budding yeast. *Genome Res.*, **31**, 411–425.
51. Romano, G.H., Harari, Y., Yehuda, T., Podhorzer, A., Rubinstein, L., Shamir, R., Gottlieb, A., Silberberg, Y., Pe'er, D., Ruppim, E. *et al.* (2013) Environmental stresses disrupt telomere length homeostasis. *PLoS Genet.*, **9**, e1003721.
52. Harari, Y. and Kupiec, M. (2018) Mec1ATR is needed for extensive telomere elongation in response to ethanol in yeast. *Curr. Genet.*, **64**, 223–234.
53. Xu, Z., Fallet, E., Paoletti, C., Fehrmann, S., Charvin, G. and Teixeira, M.T. (2015) Two routes to senescence revealed by real-time analysis of telomerase-negative single lineages. *Nat. Commun.*, **6**, 7680.
54. Coutelier, H., Xu, Z., Morisse, M.C., Lhuillier-Akakpo, M., Pelet, S., Charvin, G., Dubrana, K. and Teixeira, M.T. (2018) Adaptation to DNA damage checkpoint in senescent telomerase-negative cells promotes genome instability. *Genes Dev.*, **32**, 1499–1513.
55. Chang, M., Arneric, M. and Lingner, J. (2007) Telomerase repeat addition processivity is increased at critically short telomeres in a Tell-dependent manner in *Saccharomyces cerevisiae*. *Genes Dev.*, **21**, 2485–2494.
56. Keener, R., Connelly, C.J. and Greider, C.W. (2019) Tell activation by the MRX complex is sufficient for telomere length regulation but not for the DNA damage response in *Saccharomyces cerevisiae*. *Genetics*, **213**, 1271–1288.
57. Siede, W., Friedl, A.A., Dianova, I., Eckardt-Schupp, F. and Friedberg, E.C. (1996) The *Saccharomyces cerevisiae* Ku autoantigen homologue affects radiosensitivity only in the absence of homologous recombination. *Genetics*, **142**, 91–102.
58. Guidi, M., Ruault, M., Marbouty, M., Loiodice, I., Cournac, A., Billaudeau, C., Hoher, A., Mozziconacci, J., Koszul, R. and Taddei, A. (2015) Spatial reorganization of telomeres in long-lived quiescent cells. *Genome Biol.*, **16**, 206.
59. Batté, A., Brocas, C., Bordelet, H., Hoher, A., Ruault, M., Adjiri, A., Taddei, A. and Dubrana, K. (2017) Recombination at subtelomeres is regulated by physical distance, double-strand break resection and chromatin status. *EMBO J.*, **36**, 2609–2625.
60. Freneau, A., Santos Dos, M., Voisin, P., Tang, N., Bueno Vizcarra, M., Villagrasa, C., Roy, L., Vaurijoux, A. and Gruel, G. (2018) Relation between DNA double-strand breaks and energy spectra of secondary electrons produced by different X-ray energies. *Int. J. Radiat. Biol.*, **94**, 1075–1084.
61. Catcheside, D.G., Lea, D.E. and Thoday, J.M. (1946) The production of chromosome structural changes in *Tradescantia* microspores in relation to dosage, intensity and temperature. *J. Genet.*, **47**, 137–149.
62. Chen, C. and Kolodner, R.D. (1999) Gross chromosomal rearrangements in *Saccharomyces cerevisiae* replication and recombination defective mutants. *Nat. Genet.*, **23**, 81–85.
63. Pennaneach, V. and Kolodner, R.D. (2004) Recombination and the Tell and Mec1 checkpoints differentially effect genome rearrangements driven by telomere dysfunction in yeast. *Nat. Genet.*, **36**, 612–617.
64. Srivatsan, A., Li, B., Sanchez, D.N., Somach, S.B., da Silva, V.L., de Souza, S.J., Putnam, C.D. and Kolodner, R.D. (2019) Essential *Saccharomyces cerevisiae* genome instability suppressing genes identify potential human tumor suppressors. *Proc. Natl Acad. Sci. U.S.A.*, **116**, 17377–17382.
65. Heidenreich, E., Novotny, R., Kneidinger, B., Holzmann, V. and Wintersberger, U. (2003) Non-homologous end joining as an important mutagenic process in cell cycle-arrested cells. *EMBO J.*, **22**, 2274–2283.

66. Gangloff,S., Achaz,G., Francesconi,S., Villain,A., Miled,S., Denis,C. and Arcangioli,B. (2017) Quiescence unveils a novel mutational force in fission yeast. *eLife*, **6**, e27469.
67. Maestroni,L., Audry,J., Matmati,S., Arcangioli,B., Géli,V. and Coulon,S. (2017) Eroded telomeres are rearranged in quiescent fission yeast cells through duplications of subtelomeric sequences. *Nat. Commun.*, **8**, 1684–1614.
68. Grossi,S., Bianchi,A., Damay,P. and Shore,D. (2001) Telomere formation by Rap1p binding site arrays reveals end-specific length regulation requirements and active telomeric recombination. *Mol. Cell. Biol.*, **21**, 8117–8128.
69. Guérin,T.M., Bénéut,C., Barinova,N., López,V., Lazar-Stefanita,L., Deshayes,A., Thierry,A., Koszul,R., Dubrana,K. and Marcand,S. (2019) Condensin-mediated chromosome folding and internal telomeres drive dicentric severing by cytokinesis. *Mol. Cell*, **75**, 131–144.
70. Bonetti,D., Clerici,M., Anbalagan,S., Martina,M., Lucchini,G. and Longhese,M.P. (2010) Shelterin-like proteins and Yku inhibit nucleolytic processing of *Saccharomyces cerevisiae* telomeres. *PLoS Genet.*, **6**, e1000966.
71. Hafner,L., Lezaja,A., Zhang,X., Lemmens,L., Shyian,M., Albert,B., Follonier,C., Nunes,J.M., Lopes,M., Shore,D. *et al.* (2018) Rif1 binding and control of chromosome-internal DNA replication origins is limited by telomere sequestration. *Cell Rep.*, **23**, 983–992.
72. Wang,R., Kamgoue,A., Normand,C., Léger-Silvestre,I., Mangeat,T. and Gadal,O. (2016) High resolution microscopy reveals the nuclear shape of budding yeast during cell cycle and in various biological states. *J. Cell Sci.*, **129**, 4480–4495.
73. Ward,J.F. (1988) DNA damage produced by ionizing radiation in mammalian cells: identities, mechanisms of formation, and reparability. *Prog. Nucleic Acid Res. Mol. Biol.*, **35**, 95–125.
74. Xu,X., Nakano,T., Tsuda,M., Kanamoto,R., Hirayama,R., Uzawa,A. and Ide,H. (2020) Direct observation of damage clustering in irradiated DNA with atomic force microscopy. *Nucleic Acids Res.*, **48**, e18.
75. Toulouze,M., Amitai,A., Shukron,O., Holcman,D. and Dubrana,K. (2019) Telomeric chromosome ends are highly mobile and behave like free double-strand DNA breaks, bioRxiv doi: <https://doi.org/10.1101/720821>, 31 July 2019, preprint: not peer reviewed.
76. Tanaka,K., Kohda,A. and Satoh,K. (2013) Dose-rate effects and dose and dose-rate effectiveness factor on frequencies of chromosome aberrations in splenic lymphocytes from mice continuously exposed to low-dose-rate gamma-radiation. *J. Radiol. Prot.*, **33**, 61–70.
77. Braga-Tanaka,I., Tanaka,S., Kohda,A., Takai,D., Nakamura,S., Ono,T., Tanaka,K. and Komura,J.-I. (2018) Experimental studies on the biological effects of chronic low dose-rate radiation exposure in mice: overview of the studies at the Institute for Environmental Sciences. *Int. J. Radiat. Biol.*, **94**, 423–433.